PREPRINT STATUS STATEMENT

This is a non-peer reviewed preprint submitted to EarthArXiv. This manuscript is also currently under consideration for peer review in the journal Meteoritics & Planetary Science (Submission ID 5d2f5e85-fd7f-45fd-8b23-7499bf9d8cbc).

TITLE

Fluorapatite Breakdown and Fluor-edenite Formation in the Pristine Winonaite Calate 047 from Chile's Atacama Desert

AUTHORS AND AFFILIATIONS

Pavel Yu. Plechov [1,*], Ksenia A. Konovalova 1, Viktor M. Gekimyants[1], Vasily D. Shcherbakov[2]

[1] Fersman Mineralogical Museum, Russian Academy of Sciences, Leninsky Prospekt 18-2, Moscow, 119071, Russia

[2] Lomonosov Moscow State University, Leninskie Gory 1, Moscow, 119991, Russia

CORRESPONDING / SUBMITTING AUTHOR

Prof. Pavel Yu. Plechov

Email: pplechov@gmail.com

ORCID: 0000-0003-1086-1384

Pavel Plechov
8-12-2026

Submitted to Meteoritics&Planetary Sciences at 24 January 2026

Fluorapatite Breakdown and Fluor-edenite Formation in the Pristine Winonaite Calate 047 from Chile's Atacama Desert.

Plechov P. Yu.[1], Konovalova K. A.[1], Gekimyants V.M.[1], Shcherbakov V.D. [2]

1) Fersman Mineralogical Museum
2) Lomonosov Moscow State University

Abstract

We report the discovery and characterization of Calate 047, a new amphibole-bearing winonaite found in Chile's Atacama Desert. This meteorite exhibits a fine-grained granoblastic texture with equigranular silicates (70-350 μm) and extremely magnesian compositions (olivine $Fa_{1.6-1.8}$, low-Ca pyroxene $Wo_{1.46-1.7}Fs_{0.44-1.17}$, high-Ca pyroxene $Wo_{45.26-45.81}Fs_{0.70-0.93}$, plagioclase $An_{17.7-18.8}$). Calate 047 contains fluor-edenite amphibole (grains up to 250 μm) that lack poikilitic textures observed in previously described amphibole-bearing winonaites. Raman spectroscopy confirms the dominance of fluorine in the W-site, with characteristic peaks at 676 cm^{-1} and multiple bands between 1000-1109 cm^{-1}. Oxygen fugacity calculated from olivine composition indicates extremely reduced conditions (IW-2.7 to IW-2.8). This study establishes fluor-edenite as a systematic mineral phase in highly reduced winonaites, resolving the paradox of fluorine-rich amphibole formation in apatite-poor meteorites. We demonstrate that fluorapatite decomposition below IW-2.3 releases fluorine during reduction to schreibersite, providing the essential component for amphibole crystallization through solid-state metamorphic reactions. The absence of intermediate phosphates (merrillite, chladniite) in Calate 047 confirms direct transformation of apatite to schreibersite under extreme reduction.
As the third documented case of amphibole in winonaites, this finding provides compelling evidence for volatile-mediated metasomatism in the IAB-winonaite parent body. The correlation between amphibole occurrence and oxygen fugacity below IW-2.3 establishes a new mineralogical indicator for the most reducing conditions recorded in solar system materials, constraining redox evolution models for early planetary bodies.

Introduction

Winonaites constitute a rare group of primitive achondrites, with only 105 documented finds reported to date [Meteoritical Bulletin Database, accessed

14/12/2025]. This meteorite group is characterized by exceptionally magnesian silicates (Mg# > 95), sodic plagioclase (An < 50), abundant metallic Fe-Ni and troilite, and the presence of rare accessory minerals including phosphides, daubreelite, alabandite, and other reduced mineral phases. Winonaites share distinctive oxygen isotopic compositions with iron meteorites of the IAB group, a feature that distinguishes them from other achondrite classes [Clayton and Mayeda, 1996; Greenwood et al., 2012]. This isotopic similarity, combined with mineralogical parallels between winonaites and the silicate inclusions within IAB iron meteorites, strongly suggests a common parent body origin [Benedix et al., 2000; Bild, 1977].

Detailed studies of winonaites have revealed considerable diversity in their structural and textural features, implying a complex formation history involving their parent body [Zheng et al., 2019]. However, the classification system for primitive achondrites remains imperfect, with some meteorites potentially assigned to the winonaite group based on selected classification criteria while belonging to other groups by alternative measures. For instance, several meteorites (NWA 725, NWA 1052, NWA 1463, Dhofar 1222) contain up to 5 vol.% relict chondrules and display mineralogical characteristics typical of acapulcoites-lodranites, yet possess oxygen isotopic compositions characteristic of winonaites [Greenwood et al., 2012]. For primitive achondrites, containing relict chondrules, recently was proposed a separate group of tissemouminites [Stefant et al., 2023] and they are thought to originate from a distinct parent body, different from the winonaite parent body. Presently, some of these meteorites are classified as winonaites while others are designated as acapulcoites or lodranites [Meteoritical Bulletin Database, accessed 14/12/2025]. This classification ambiguity underscores the need for multiple criteria including structural, textural, mineralogical, and isotopic parameters in the proper categorization of these complex meteorites.

Winonaites have undergone thermal metamorphism up to partial melting of metal and sulfides [Benedix et al., 2005; Hunt et al., 2017; Zeng et al., 2019; Anzures et al., 2024]. The temperature range for silicate paragenesis formation (900-1200°C) [Benedix et al., 2005] is significantly higher than temperature estimates for tissemouminites (approximately 820°C) [Stefant et al., 2023], which should result in textural differences. Genuine high-temperature winonaites could not retain relict chondrules but instead developed granoblastic structures similar to those of petrologic types 6-7.

Winonaite formation occurred under extremely reducing conditions, several orders of magnitude below the IW (iron-wüstite) buffer. This leads to apatite instability and the appearance in winonaites (and IAB iron meteorites) of extremely rare phosphates: morascoite ($Na_2Mg[PO_4]F$), chladniite ($Na_2CaMg_7[PO_4]_6$), kryzaite ($Na_4(Mg, Cr)[PO_4]_3$) and chzochralskiite ($Na_4Ca_3Mg[PO_4]_4$), followed by the iron phosphide schreibersite (Fe3P). Fluor-edenite amphibole ($NaCa_2Mg_5[Si_7Al]O_{22}F_2$) has been described in two winonaites [Floss et al., 2007; Carpenter et al., 2021], a mineral that is extremely rare in meteoritic material. We have also discovered fluor-edenite in the recently found winonaite Calate 047. This third discovery of fluor-edenite in winonaites indicates that its presence in meteorites of this type represents a systematic feature rather than an anomaly. In this article, we present a description of the Calate 047 winonaite, report results of fluor-edenite investigation, and propose a mechanism for fluor-edenite formation involving apatite under extremely low oxygen fugacity conditions.

Samples and Methods

The meteorite, weighing approximately 0.8 g, was discovered by V.M. Gekimyants in November 2023 in the Atacama Desert, Chile, and was officially registered in September 2024. The registered mass and thin section are housed in the collection of the Fersman Mineralogical Museum of the Russian Academy of Sciences as winonaite Calate 047 (collection number FMM_10_272; thin section number 2097 in the Museum's thin section collection, corresponding to number FN1110 in the research collection).

Mineral compositions and elemental mapping of specific thin section areas were determined using energy-dispersive electron probe microanalysis (Oxford X-MaxN spectrometer with an 80 mm² crystal area, mounted on a JEOL JSM-IT500 scanning electron microscope) at the Laboratory of Analytical Techniques of High Spatial Resolution, Department of Petrology and Volcanology, Geological Faculty, Moscow State University. Analyses were conducted at an accelerating voltage of 20 kV and a probe current of 0.7 nA. Additional studies were performed using a TESCAN MIRA3 Imh scanning electron microscope equipped with an Oxford Ultimax EDS detector at the Analytical Department of the Shared Research Center of the Geochemistry Institute, Siberian Branch, Russian Academy of Sciences. Raman spectra were obtained using an EnSpectr R532

Raman attachment mounted on an Olympus BX53 microscope, equipped with a 532 nm laser. Spectra were acquired in the range of 150-1200 cm^{-1}. To verify the absence of water in amphibole, measurements were also conducted in the 3200-3600 cm^{-1} range, but no O-H vibrational bands were detected. Spectra were processed using the web application ArDi [Shendrik et al., 2024].

Results

The Calate 047 winonaite exhibits a fine-grained granoblastic texture, with the predominant grain size ranging from 70 to 350 μm. Clinopyroxene and plagioclase grains display a narrower size distribution, not exceeding 150 μm. The meteorite is traversed by a network of cracks 10–50 μm in thickness, filled with iron oxides that formed during terrestrial weathering.

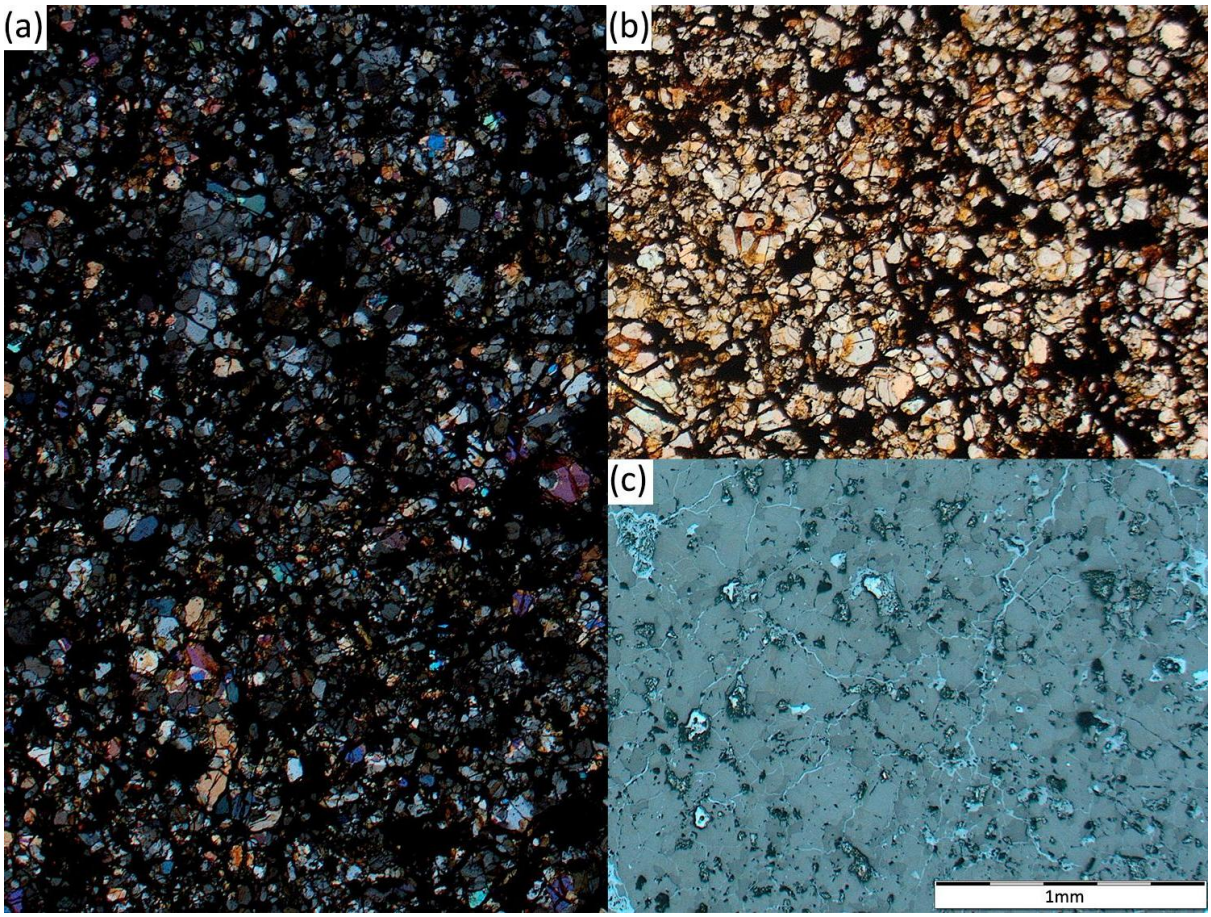

Fig. 1. General view of the Calate 047 winonaite in thin section: a) cross-polarized light, b) under plane-polarized light, c) reflected light without analyzer.

The Calate 047 winonaite is predominantly composed of low-calcium pyroxene, with minor amounts of olivine, high-calcium pyroxene, plagioclase, and fluor-

edenite (Fig. 1 and 2). Intense terrestrial weathering has led to the replacement of primary sulfides and metallic phases: only isolated relict grains of taenite ((Fe,Ni)), schreibersite ($(Fe,Ni)_3P$), and troilite (FeS), measuring up to 40 μm, are preserved within cracks and interstices of the silicate matrix (Fig. 1c).

The chemical composition of the rock-forming minerals (Table 1) is more magnesian compared to other described fluor-edenite-bearing winonaites (Floss et al., 2007; Carpenter et al., 2021) and corresponds to olivine $Fa_{1.6\text{-}1.8}$, Low-Ca pyroxene $Wo_{1.46\text{-}1.7}Fs_{0.44\text{-}1.17}$, and Ca-pyroxene $Wo_{45.26\text{-}45.81}Fs_{0.70\text{-}0.93}$. Plagioclase in the meteorite is represented by oligoclase with $An_{17.7\text{-}18.8}$.

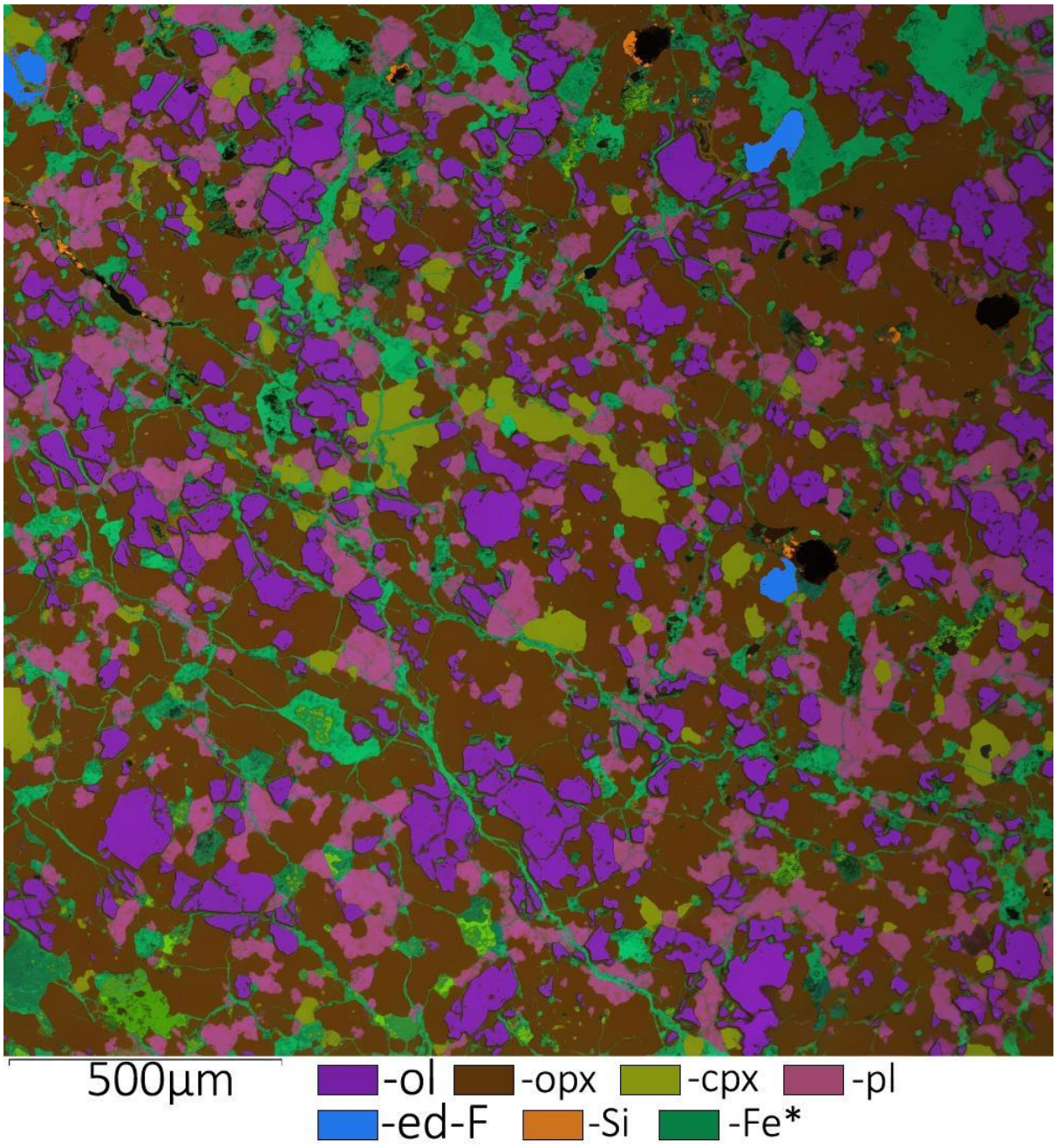

Fig. 2. Phase distribution within a fragment of thin section FN1110 from the Calate 047 winonaite. Opx – low-Ca pyroxene, Cpx – high-Ca pyroxene, Ol – olivine, Pl – plagioclase, Ed-F – fluoro-edenite, Fe* – iron hydroxides (terrestrial weathering products), Si – silica.

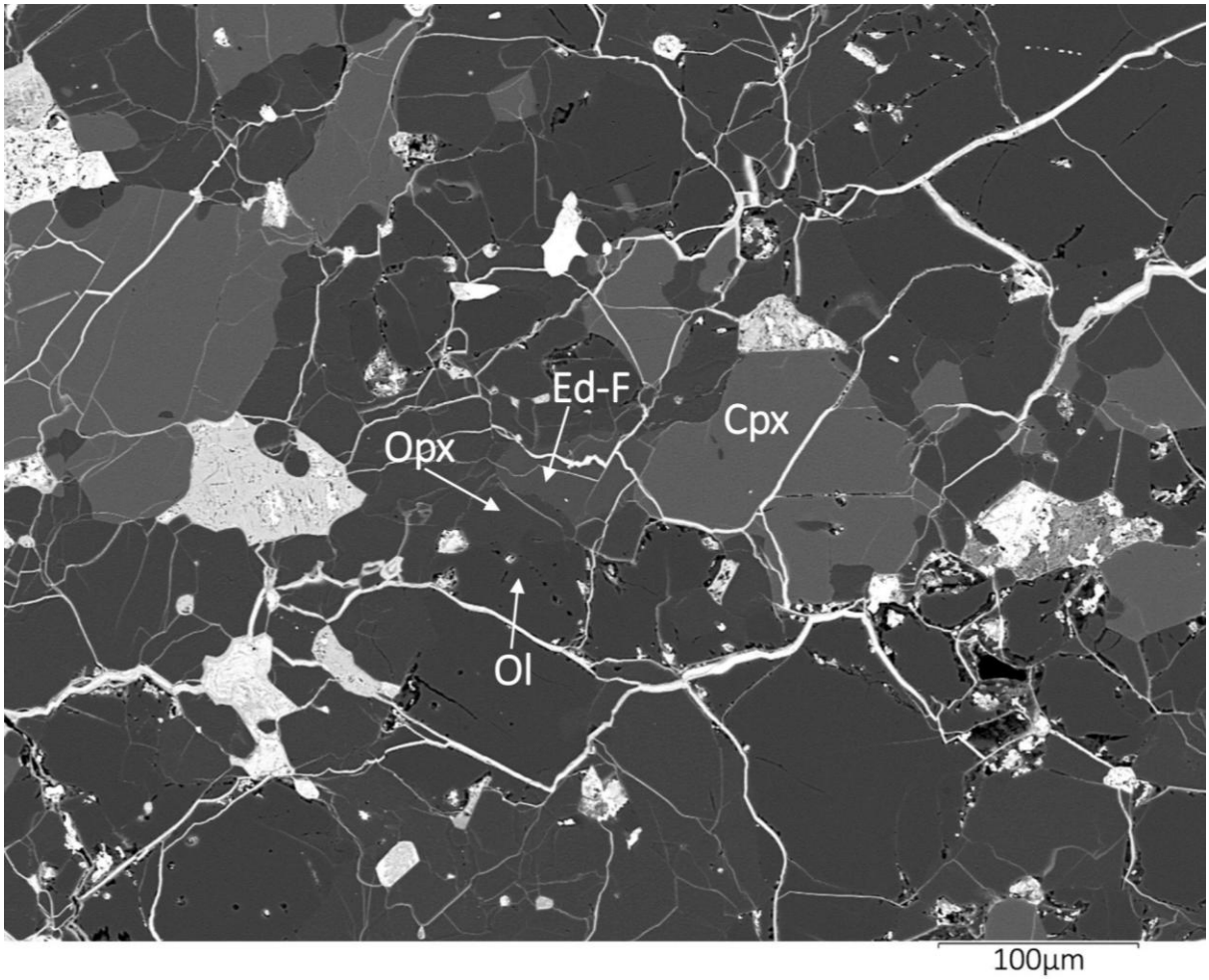

Fig. 3. BSE image of an amphibole-bearing area. Mineral abbreviations are identical to those in Fig. 2.

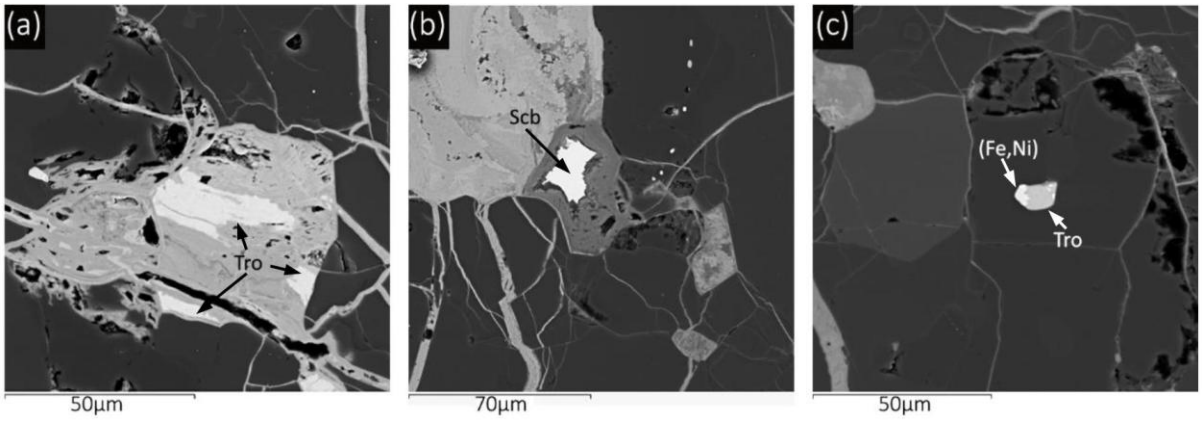

Fig. 4. BSE images of relict grains preserved among weathering products: troilite (Tro) (a), schreibersite (Scb) (b), and taenite (Fe,Ni) (c).

The chemical compositions of the rock-forming minerals are provided in Table 1 and in the Supplementary Materials.

TABLE 1. Major element composition (wt%) in Calate 047 minerals.

	Low-Ca pyroxene	Ca-pyroxene	Olivine	Plagioclase
	n=6	n=6	n=7	n=5
SiO_2	58.09	54.17	41.70	61.94
TiO_2	0.13	0.53	n.d.	n.d.
Al_2O_3	1.07	1.86	0.05	24.10
Cr_2O_3	0.13	0.20	0.03	n.d.
FeO	1.27	0.55	1.70	0.33
MnO	0.24	0.15	0.17	0.06
MgO	37.85	18.95	55.73	n.d.
CaO	0.87	22.46	0.03	3.71
Na_2O	0.03	0.41	n.d.	8.82
K_2O	n.d.	n.d.	n.d.	0.46
NiO	n.d.	n.d.	0.02	n.d.
Total	99.68	99.26	99.43	99.42
This work	$Wo_{1.46\text{-}1.7}Fs_{0.44\text{-}1.17}$	$Wo_{45.26\text{-}45.81}Fs_{0.70\text{-}0.93}$	$Fa_{1.6\text{-}1.8}$	$An_{17.7\text{-}18.8}$
Floss et al., 2007(HaH 193)	$Wo_{1.7\text{-}2.0}Fs_{4.9\text{-}5.1}$	$Wo_{43.2–44.2}Fs_{1.3–2.2}$	$Fa_{4.3\ –\ 4.6}$	$An_{20.9–21.4}$
Carpenter et al., 2021 (NWA 13432)	$Wo_{1.7\text{-}\ 1.9}Fs_{3.5\text{-}3.8}$	$Wo_{44.8\text{-}45.8}Fs_{1.1\text{-}1.3}$	$Fa_{3.0\text{-}3.3}$	$An_{20.8}$

Fluor-edenite grains do not exceed 250 μm in size and form part of a granoblastic aggregate (Fig. 2, 3 and 5). Unlike fluor-edenite reported in previous studies [Floss et al., 2007; Carpenter et al., 2021], the grains of this mineral in Calate 047 are characterized by smaller dimensions (approximately 200 μm versus 1–2 mm) and lack poikilitic inclusions of fine-grained phases (Fig. 5).

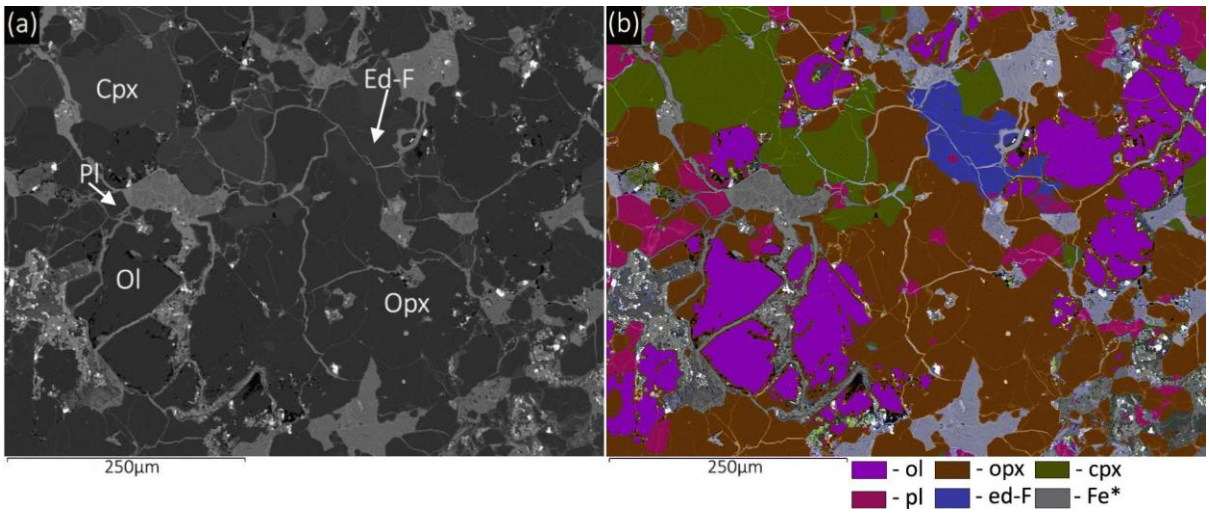

Fig. 5. BSE image (a) and phase map (b) of an amphibole-bearing region in the thin section, showing a small plagioclase inclusion (blue in phase map) within a fluor-edenite grain.

The calculation of the fluor-edenite formula (as with other amphiboles) involves several assumptions. In this case, we consider all iron and manganese in the amphibole to be divalent, and titanium to be tetravalent, since the oxygen fugacity for winonaites is estimated at the IW-2.5 oxygen buffer level [Benedix et al., 2005]. For the calculation, we used the method of normalization to 15 cations. Cation site allocation was performed according to the recommendations for cation distribution in amphiboles (Hawthorne et al., 2012). We considered all anion sites to be fully occupied (22 oxygen atoms and 2 sites for F, Cl, OH, or O). Vacancies in cation sites were assigned to the A-site (sum of Na+K < 1). The total cation sum in the studied amphibole is approximately 15.6, and the difference from the 16 cations in the theoretical edenite formula can be explained by an intermediate composition between edenite and tremolite. All calcium (1.7-1.8 a.p.f.u.) occupies the B-site, and the deficiency in the B-site is compensated by an excess of cations in the C-site (5.2-5.3 a.p.f.u.), indicating the possible presence of a cummingtonite component. In the studied amphibole, the sum of Fe+Mn does not exceed 0.1 a.p.f.u., and complete assignment of these elements to the B-site is not meaningful. Fluorine (1.8-1.9 a.p.f.u.) almost entirely occupies

the W-site. The F/Cl ratio in the amphibole exceeds 100. The sum of cation charges ranges from 46.1 to 46.2, whereas the sum of anion charges is 45.8-45.9. This difference can be compensated if the remaining portion of the W anion site is filled with oxygen atoms rather than hydroxyl groups. This is consistent with the absence in Raman and IR spectra of bands corresponding to O-H vibrations in the range 3200-3600 cm^{-1}. Thus, the formula of the studied amphibole can be written as:

$(Na_{0.55-0.58},K_{0.05-0.06})_{0.60-0.64}Ca_{1.72-1.8}(Mg_{4.88-5.09}Fe^{2+}_{0.05-0.09}Al_{0.00-0.19}Ti^{4+}_{0.06-0.11}Cr_{0.01}Mn_{0.00-0.01})_{5.20-5.28}(Si_{7.30-7.52}Al_{0.48-0.67}Ti^{4+}_{0.00-0.06})_8O_{22}(F_{1.79-1.85}Cl_{0.01-0.02}O_{0.13-0.38})_2$

Based on its composition, the amphibole corresponds to fluoro-edenite, as fluorine clearly dominates the W-site over other anions, magnesium predominates in the C-site, and the sum of Na+K exceeds the number of vacancies in the A-site.

The Raman spectrum of the analyzed fluoro-edenite grains is presented in Fig. 6, compared with reference spectra of terrestrial edenite from Mogok, Burma (RRUFF database, R050415) and Pargas fluoro-edenite (Fersman Mineralogical Museum of the Russian Academy of Sciences, sample FMM_1_92056). A clear correspondence is observed for the primary vibration band characteristic of the edenite-pargasite subgroup at approximately 676 cm^{-1}, as well as for the group of bands in the 1000–1100 cm^{-1} range [Apopei & Buzgar, 2010]. Table 2 shows a comparison of the main vibrational bands for fluoro-edenite found in winonaites (this study and [Floss et al., 2007]) with terrestrial fluoro-edenite samples [Rinaudo et al., 2006].

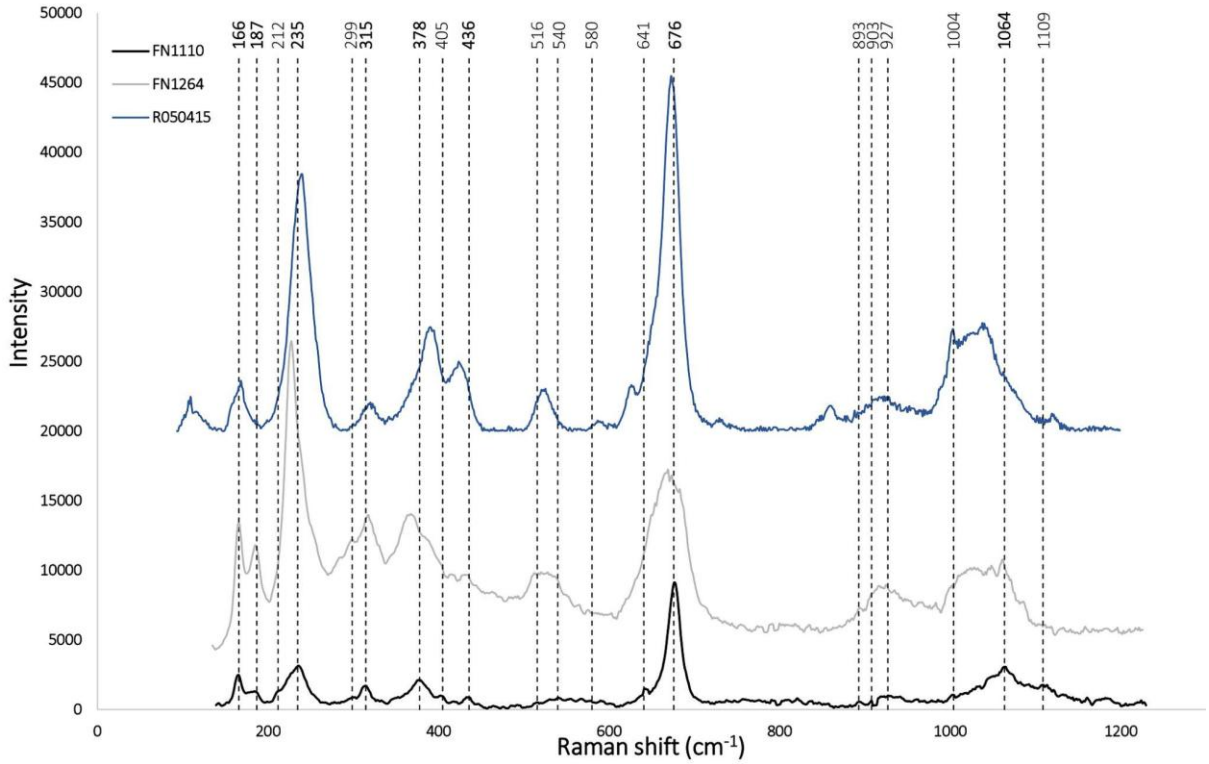

Fig. 6. Comparison of Raman spectra of fluoro-edenite from the Calate 047 winonaite (FN1110) with a reference sample from the Fersman Mineralogical Museum (FN1264) and edenite from the RRUFF database (R050415).

The most intense peak at 676 cm^{-1} with a shoulder at 641 cm^{-1} corresponds to the symmetric ν_1 vibration of Si-O_β-Si bonds and is consistent with data from [Rinaudo et al., 2006] and the reference sample. The presence of the shoulder is attributed to significant aluminum content in tetrahedral sites. In the 1000–1109 cm^{-1} region, bands at 1004, 1064, and 1109 cm^{-1} are assigned to asymmetric vibrations (ν_{as}) of Si-O_β-Si bonds. Peaks at 893, 908, and 927 cm^{-1} correspond to symmetric vibrations (ν_s) of O-Si-O bonds. The group of bands between 160–300 cm^{-1} is associated with lattice vibrations. Weak bands at 514, 540, and 580 cm^{-1} may be related to deformation vibrations of the Si_4O_{11} tetrahedral group [Apopei & Buzgar, 2010]. Bands at 405 and 436 cm^{-1} are attributed to M-O vibrations in octahedral sites, where M represents Ca^{2+} and Mg^{2+}. Bands at 315 and 378 cm^{-1} can be interpreted as M-F bonds [Della Ventura et al., 2021].

TABLE 2. Wavenumbers and assignments for the Raman spectra of the flouro-edenite sample in the 150- 1200 cm^{-1} spectral region

Floss et al., 2007	Rinuado et al., 2006	This study	Bonds
		1109	ν_{as} in
1067	**1061**	**1064**	Si-O_b-Si
	1041	1004	
926	929	927	ν_s in
		908	Si-O-Si
	899	893	
	760		? ν_s in Si-O_b-Si
679	**679**	**676**	ν_s in Si-O_b-Si(ν_1)
		641	
	587	580	breathing of
	557	540	Si_4O_{11}
	528	516	
	435	436	M-O, where
		405	M=Ca and
382	**382**	**378**	Mg
	370		
315	**312**	**315**	
		299	low-frequency vibrations
	258		
	249		
	238	**235**	
228	225		
		212	
185		**187**	
		166	

Discussion

The classification of primitive achondrites has developed since the early 20th century [Prior, 1916]. The grouping of four meteorites, namely Kakangari, Mt. Morris (Wisconsin), Pontlyfni, and Winona, into a separate category termed “forsterite chondrites” was proposed in [Graham et al., 1977]. The Kakangari

meteorite was subsequently assigned to an independent group of K-chondrites [Weisberg et al., 1996]. The identification of winonaites as a distinct group among primitive achondrites, defined by the presence of highly magnesian silicates, was introduced in [Prinz et al., 1980]. This group initially encompassed not only Winona, Mt. Morris, and Pontlyfni but also the meteorites Acapulco and ALHA77081. Acapulco and ALHA77081 were later reclassified into the acapulcoite group because their clinopyroxene contains more than 1 wt.% Cr_2O_3 and they exhibit other significant differences from winonaites [Kimura et al., 1992]. During this period, accumulated data on oxygen isotopic compositions facilitated the development of a unified classification system for achondrites [Clayton & Mayeda, 1996]. Acapulcoites and lodranites share identical oxygen isotopic signatures and were combined into the acapulcoite-lodranite group, whereas winonaites display oxygen isotopic compositions closest to those of silicate inclusions in IAB iron meteorites. However, classification based exclusively on oxygen isotopes frequently conflicts with structural, textural, and mineralogical distinctions among different groups. For instance, meteorites such as Dhofar 1222, NWA 725, NWA 1463, NWA 1052, NWA 1054, NWA 1058, and NWA 8614, classified by oxygen isotopic composition as winonaites or acapulcoites (i.e., achondrites), contain substantial amounts of chondrules. Recently, such meteorites have been proposed for inclusion in a separate group called tissemouminites [Stephant et al., 2023]. Texturally, they resemble type 6 chondrites, while their oxygen isotopic compositions fall between those of acapulcoites and winonaites.

Oxygen isotope fractionation can occur not only through mass-dependent scenarios [Clayton, 2008]. It has been experimentally and theoretically demonstrated that ozone molecules become enriched in heavy oxygen isotopes due to molecular asymmetry [Thiemens and Heidenreich, 1983; Gao and Marcus, 2002]. Additionally, oxygen isotope fractionation is considered during photochemical effects involving CO molecules [Lyons and Young, 2005]. Given that winonaite formation is thought to involve destruction and reassembly of the parent body in meteorites of this group [Zeng et al., 2019], isotopic heterogeneity may arise, including through mixing with an external source enriched in ^{16}O. Therefore, we prefer to determine meteorite classification within the winonaite group not solely based on oxygen isotopes, but also using structural, textural, mineralogical, and petrological criteria. Proper winonaites belong to achondrites, meaning they should not contain chondrules. They exhibit granoblastic medium-grained structures corresponding to thermal metamorphism at 800-1100°C. They

are characterized by extremely magnesian silicate compositions (Mg# > 95), high modal content of metal and troilite, and the presence of rare phosphates, phosphides, daubreelite, and alabandite, reflecting extremely reduced crystallization conditions [Benedix et al., 1998].

Of particular interest for discussion is the discovery of fluorine-dominant amphibole in meteoritic material. This represents the third documented occurrence of amphibole in winonaites, suggesting its presence in meteorites of this type is systematic rather than anomalous. Grains of fluorine-dominant amphibole, besides those found in the Calate 047 winonaite studied here, have been described in the winonaites NWA 13432 [Carpenter et al., 2021] and HaH 193 [Floss et al., 2007], and have also been noted in the winonaites NWA 16875, NWA 13968, NWA 15866, and NWA 14558 (MetBull database). Additionally, fluorine-bearing amphiboles have been reported in IAB iron meteorites Wichita County and Canyon Diablo [Olsen et al., 1973], the EH4 enstatite chondrite Abee [Douglas and Plant, 1968], and the aubrite Mayo Belwa [Bevan et al., 1977]. Common characteristics of these occurrences include: 1) extremely high magnesian content of silicates; 2) high modal abundance of orthopyroxene; 3) presence of metal. Winonaites are associated with the parent body of IAB meteorites [Benedix et al., 2000], whereas no such connection is proposed for enstatite chondrites and aubrites.

In all three described amphibole-bearing winonaites, the amphibole composition is remarkably similar. It is fluor-edenite with high fluorine content (3.99–4.56 wt.%) and low chlorine content (0.03–0.07 wt.%). The molecular F/Cl ratio exceeds 100. Neither hydroxyl groups nor molecular water were detected in any of the studied samples. The average magnesian content (100×Mg/(Mg+Fe), mol.%) of fluor-edenite in Calate 047 is 98.7 (n=5), in NWA 13432 it is 98.2 (n=53), and in HaH 193 it is 97.1 (n=17), which correlates well with the magnesian content of other silicates in these meteorites (see table 1). The Al_2O_3 content is directly proportional to magnesium content, ranging from 5.9 to 7.7 wt.%. Titanium varies within narrow limits of 1.0–1.1 wt.% TiO_2. Chromium content is inversely proportional to magnesium content—its minimum (0.21 wt.% Cr_2O_3, n=5) was recorded in Calate 047 fluor-edenite, while the maximum was found in HaH 193 (0.62 wt.% Cr_2O_3, n=17).

The reported amphibole compositions in IAB iron meteorites [Olsen et al., 1973] differ significantly from those in winonaites. These amphiboles exhibit substantially lower Al_2O_3 content (up to 0.4 wt.%) and higher silica content, corresponding not to fluor-edenite but to fluor-richterite. They also show elevated

TiO_2 (1.5–2.2 wt.%) and Cr_2O_3 (up to 3.5 wt.%), with K_2O reaching up to 1.2 wt.%. The reported fluorine content ranges from 2.3 to 3.6 wt.%, which is lower than in winonaite amphiboles. Chlorine content was not provided in the published analyses. Fluor-richterite from the Abee enstatite chondrite resembles amphiboles from IAB meteorites but contains virtually no titanium or aluminum. Nevertheless, it displays the highest magnesian content (99.6 mol.%) among all amphiboles described in meteorites [Olsen et al., 1973].

Amphibole is an exceptionally rare mineral in meteorites, indicative of specific formation conditions. The granoblastic texture of the Calate 047 winonaite, with uniformly distributed grains 70–120 μm in size, suggests formation under near-equilibrium conditions, excluding crystallization from melt as a mechanism for fluor-edenite formation. This textural observation, combined with the absence of silicate melt features, supports an origin for the amphibole through metamorphic or metasomatic processes. It is critically important to note that the granoblastic texture of Calate 047 reflects a prolonged recrystallization process at temperatures below the melting point of silicates yet sufficient for volatile diffusion (600–800°C) [Benedix et al., 2005]. This mechanism differs fundamentally from shock-induced amphibole formation observed in the Mayo Belwa aubrite, where needle-like richterite crystals develop in cavities during short-duration high-temperature pulses [Graham et al., 1977a].

Two distinct temperature intervals reflecting the formation history of winonaites have been identified [Benedix et al., 2005]. The first interval, calculated using the two-pyroxene geothermometer [Kretz, 1981], corresponds to a range of 913–1084°C, while the second interval (586–700°C) represents the closure temperature of the olivine-chromite exchange reaction. For the Calate 047 meteorite, the temperature estimated from the two-pyroxene equilibrium [Kretz, 1981] is 1104°C. Using the olivine-clinopyroxene geothermometer [Loucks, 1996], a temperature of 1181°C was calculated.

We applied the oxygen fugacity calculation scheme based on silicate compositions in equilibrium with metallic iron, as proposed by [Benedix et al., 2005], which relies on the reaction governing the QIF (quartz-iron-fayalite) oxygen buffer:

$$Quartz + 2Fe + O_2 = Fayalite$$

By expanding equation 3 from [Benedix et al., 2005] and applying the fixed activity values provided in that study (a_{Fe} = 0.91 and a_{SiO2} = 0.9), we derive a

simplified formula for oxygen fugacity as a function of temperature and the activity of the fayalite component in olivine:

$$\log (fO_2) = 29482/T + 7.56 + \log(a_{Fa})$$

Given that the olivine solid solution approximates ideal behavior [Sack and Ghiorso, 1989], we can adopt $a_{Fa} = X_{Fa} = 1 - X_{Fo}$. At a fixed temperature, higher magnesium content of silicates in equilibrium with metal reflects more reduced conditions. This equation can be reformulated relative to the IW (iron-wüstite) oxygen buffer when temperature is fixed (e.g., at 1000°C):

$$\Delta IW = -0.99 + \log(x_{Fa})$$

This equation demonstrates that the QIF oxygen buffer is close to IW-1 (at $X_{Fa} = 1$), and a shift toward more reducing conditions relative to this buffer is reflected in a decrease in the fayalite content of olivine. At QIF-1 (IW-2), olivine will have a composition of $Fo_{90}Fa_{10}$, and at QIF-2 (IW-3) – $Fo_{99}Fa_{1}$.

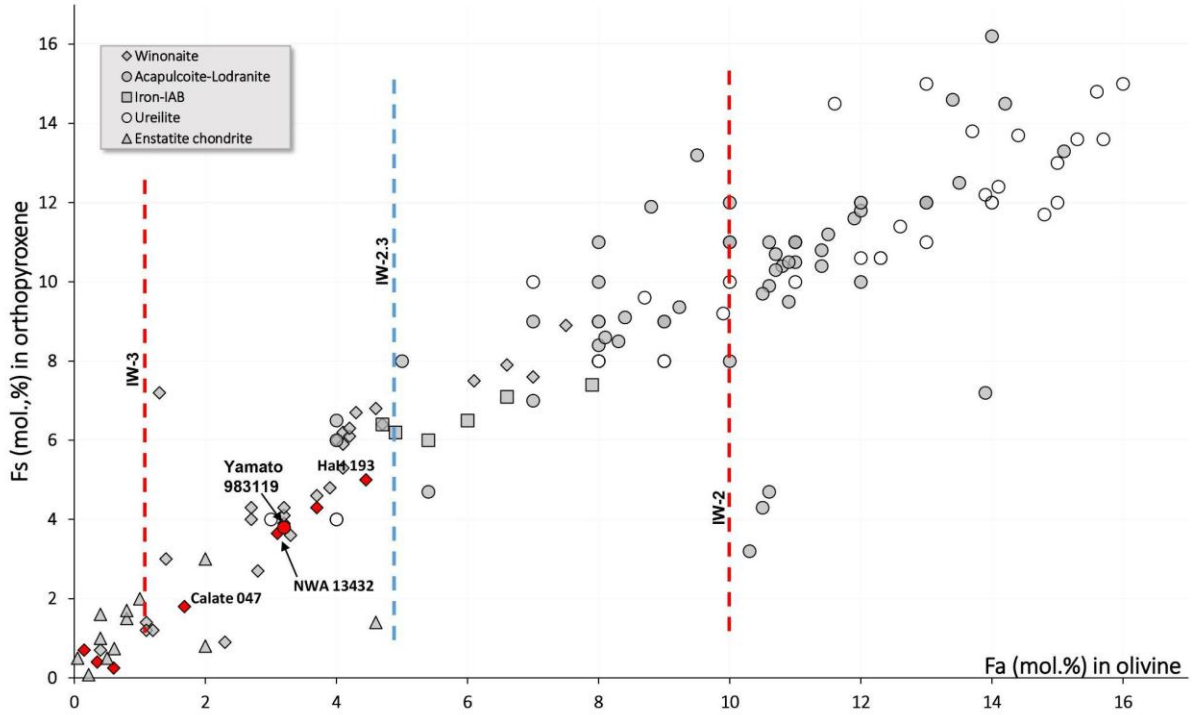

Fig. 7. Fa content (in olivine) and Fs content (in orthopyroxene) for various meteorite types. Meteorites (winonaites and lodranites) in which amphiboles have been described are highlighted in color. Mineral chemical composition data are taken from [Benedix et al., 2005; Carpenter et al., 2021; Floss et al., 2007; Yasutake et al., 2017] and from the MetBull database.

Olivine in the Calate 047 meteorite has a composition of Fa1.6-1.8, corresponding to an oxygen fugacity at the IW-(2.7-2.8) buffer level. Figure 7 displays silicate compositions in primitive achondrites, enstatite chondrites, iron meteorites, and ureilites. The magnesium content of silicates directly correlates with oxygen fugacity. The position of lines relative to the IW oxygen buffer was calculated using the fayalite equilibrium equation presented above. Meteorites in which fluoro-edenite has been identified are highlighted with colored symbols. All descriptions of fluoro-edenite (except for meteorite Yamato 983119, classified as a lodranite based on oxygen isotopic composition) pertain to winonaites. In meteorite Yamato 983119, fluorine-rich amphibole and biotite occur as intergrowths with each other and potassium feldspar, and are interpreted as melt inclusions within orthopyroxene [Yasutake and Yamaguchi, 2017]. It is proposed that fluorine migrated through cracks into these inclusions during metasomatic processing after crystallization [Yasutake and Yamaguchi, 2017].

A reaction between clinopyroxene and plagioclase in the presence of fluorine has been proposed for fluoro-edenite formation in winonaites [Floss et al., 2007]:

$$MgCaSi_2O_6\ (Di)+NaAlSi_3O_8(Ab)+2Mg_2SiO_4(Ol)+CaF_2=NaCa_2Mg_5AlSi_7O_{22}F_2$$

The fluorine source in this process is a Ca- and F-enriched fluid produced by the decomposition of fluorapatite. Apatite in primitive achondrites, including winonaites, is predominantly fluorapatite with a composition close to $Ca_5(PO_4)_3F$, containing Cl <0.3 wt.% and OH <0.1 wt.% [Buseck and Steele, 1988]. At oxygen fugacities below the IW-2.4 buffer (characteristic of the IAB-winonaite complex [Benedix et al., 2005]), fluorapatite becomes thermodynamically unstable. Experimental data demonstrate that under low oxygen fugacity conditions, phosphates (whitlockite) can transform into iron phosphides (schreibersite) [Pasek, 2017]. The calculated whitlockite-schreibersite buffer has an oxygen fugacity approximately 1 log unit lower than the conditions recorded in winonaites [Anzures et al., 2024].

We can assess apatite stability in winonaites under the assumption that apatite serves as the fluorine source during fluoro-edenite formation. Figure 7 demonstrates that amphibole appears at oxygen fugacities below IW-2.3, which likely represents the lower stability boundary of apatite. It should be noted that both the absolute oxygen fugacity and the position of the schreibersite-whitlockite buffer relative to the IW buffer are temperature-dependent. Figure 7

is calculated for a temperature of 1000°C. At lower equilibrium temperatures, apatite decomposition would require even lower oxygen fugacity (or a greater deviation from the IW buffer). Apparently, winonaites developed optimal conditions for amphibole formation: high-temperature metamorphism accompanied by reduction processes. Prior to this stage, fluorapatite persisted as the primary fluorine reservoir. In these meteorites, it transformed directly into schreibersite, bypassing the intermediate stage of anhydrous phosphate formation (merrillite, chladniite, etc.). In the studied Calate 047 meteorite, neither apatite nor other phosphates were found, but schreibersite was identified, confirming the mechanism previously proposed [Floss et al., 2007]. It would be instructive to examine other winonaites with calculated oxygen fugacities below the IW-2.3 level (olivine magnesian content >95%) for the presence of amphibole, apatite, schreibersite, and rare phosphates. Such an investigation might reveal incomplete amphibole-forming reactions with relict apatite grains, providing an opportunity to refine amphibole formation mechanisms and gain further insights into the evolution of the winonaite parent body. We believe that amphibole represents a typical accessory mineral in winonaites, as its occurrence consistently follows from the mineralogy of winonaites and their extremely reduced crystallization conditions.

Conclusion

The discovery of fluor-edenite amphibole in the newly found Calate 047 winonaite from Chile's Atacama Desert provides compelling evidence that amphibole formation is a systematic feature rather than an anomaly in winonaites formed under extremely reducing conditions. This meteorite records high-temperature metamorphism (900–1180°C) under exceptionally low oxygen fugacity conditions (IW-2.7 to IW-2.8) in the IAB-winonaite parent body, evidenced by its granoblastic texture, exceptionally magnesian silicates (Fa1.6–1.8), and absence of primary phosphates.

The formation of fluor-edenite in winonaites is directly linked to the thermodynamic instability of fluorapatite under extremely reducing conditions (oxygen fugacity below IW-2.3). At metamorphic temperatures of 900–1180°C, fluorapatite decomposes as the IAB-winonaite parent body undergoes progressive reduction, releasing fluorine into the system while phosphate components are reduced to schreibersite. This mechanism, now documented in three independent winonaite samples, establishes fluorapatite decomposition as a systematic pathway for amphibole genesis in reduced primitive achondrites. The

presence of fluor-edenite provides a new mineralogical indicator for extremely reducing environments in the early solar system.
Future studies of additional amphibole-bearing winonaites may reveal intermediate reaction stages with relict apatite, further refining our understanding of reducing processes and volatile cycling during parent body metamorphism.

Acknowledgments

This work was supported by the state budget project FMWF-2025-0003 "Species and chemical diversity of minerals and their parageneses in terrestrial and meteoritic matter" of the Fersman Mineralogical Museum of the Russian Academy of Sciences. English text editing was performed with QWEN3-Max.

Literature

Anzures, B. A., McCubbin, F. M., Erickson, T. M., Jakubek, R. S., Fries, M. D., & Le, L. (2024). First widespread occurrence of rare phosphate chladniite in a meteorite, winonaite Graves Nunataks (GRA) 12510: Implications for phosphide–phosphate redox buffered genesis in meteorites. American Mineralogist, 109(9), 1513-1522.

Apopei, A. I., & Buzgar, N. (2010). The Raman study of amphiboles. Analele Stiintifice de Universitatii AI Cuza Din Iasi. Sect. 2, Geologie, 56(1), 57.

Benedix, G. K., McCoy, T. J., Keil, K., Bogard, D. D., & Garrison, D. H. (1998). A petrologic and isotopic study of winonaites: Evidence for early partial melting, brecciation, and metamorphism. *Geochimica et Cosmochimica Acta*, *62*(14), 2535-2553.

Benedix, G. K., McCoy, T. J., Keil, K., & Love, S. G. (2000). A petrologic study of the IAB iron meteorites: Constraints on the formation of the IAB-Winonaite parent body. Meteoritics & Planetary Science, 35(6), 1127-1141.

Benedix, G. K., Lauretta, D. S., & McCoy, T. J. (2005). Thermodynamic constraints on the formation conditions of winonaites and silicate-bearing IAB irons. *Geochimica et Cosmochimica Acta*, *69*(21), 5123-5131.

Bild, R. W. (1977). Silicate inclusions in group IAB irons and a relation to the anomalous stones Winona and Mt Morris (Wis). *Geochimica et Cosmochimica Acta, 41(10),* 1439-1456.

Carpenter, P., Irving, A., & Jolliff, B. (2021). EPMA of amphibole in meteorites: Nakhlite northwest Africa 13368 and Winonaite northwest Africa 13432. *Microscopy and Microanalysis*, *27*(S1), 2796-2798.

Clayton, R. N., & Mayeda, T. K. (1996). Oxygen isotope studies of achondrites. *Geochimica et Cosmochimica Acta, 60(11)*, 1999-2017.

Della Ventura, G., Hawthorne, F. C., Mihailova, B., & Sodo, A. (2021). Raman and FTIR spectroscopy of synthetic amphiboles: I. The OH librational bands and the determination of the OH-F content of richterites via Raman spectroscopy. The Canadian Mineralogist, 59(1), 31-41.

Floss, C., Jolliff, B. L., Benedix, G. K., Stadermann, F. J., & Reid, J. (2007). Hammadah al Hamra 193: The first amphibole-bearing winonaite. American Mineralogist, 92(4), 460–467. doi:10.2138/am.2007.2253

Gao, Y. Q., & Marcus, R. A. (2002). On the theory of the strange and unconventional isotopic effects in ozone formation. The Journal of chemical physics, 116(1), 137-154.

Graham, A. L., Easton, A. J., & Hutchison, R. (1977a). The Mayo Belwa meteorite: a new enstatite achondrite fall. Mineralogical Magazine, 41(320), 487-492.

Graham, A. L., Easton, A. J., & Hutchison, R. (1977b). Forsterite chondrites; the meteorites Kakangari, Mount Morris (Wisconsin), Pontlyfni, and Winona. Mineralogical Magazine, 41(318), 201-210.

Greenwood, R. C., Franchi, I. A., Gibson, J. M., & Benedix, G. K. (2012). Oxygen isotope variation in primitive achondrites: The influence of primordial, asteroidal and terrestrial processes. *Geochimica et Cosmochimica Acta, 94*, 146-163.

Hawthorne, F. C., Oberti, R., Harlow, G. E., Maresch, W. V., Martin, R. F., Schumacher, J. C., & Welch, M. D. (2012). Nomenclature of the amphibole supergroup. *American Mineralogist*, *97*(11-12), 2031-2048.

Kimura, M., Tsuchiyama, A., Fukuoka, T., & Iimura, Y. (1992). Antarctic primitive achondrites Yamato-74025,-75300, and-75305: Their mineralogy, thermal history and the relevance to winonaite. In Proceedings of the NIPR Symposium on Antarctic Meteorites (Vol. 5, pp. 165-190). National Institute of Polar Research.

Kretz, R. (1982). Transfer and exchange equilibria in a portion of the pyroxene quadrilateral as deduced from natural and experimental data. Geochimica et Cosmochimica Acta, 46(3), 411-421.

Loucks, R. R. (1996). A precise olivine-augite Mg-Fe-exchange geothermometer. Contributions to Mineralogy and Petrology, 125(2), 140-150.

Lyons, J. R., & Young, E. D. (2005). CO self-shielding as the origin of oxygen isotope anomalies in the early solar nebula. Nature, 435(7040), 317-320.

Olsen, E., Huebner, J. S., Douglas, J. A. V., & Plant, A. G. (1973). Meteoritic amphiboles. American Mineralogist: Journal of Earth and Planetary Materials, 58(9-10), 869-872.

Pasek, M. A. (2017). Schreibersite on the early Earth: scenarios for prebiotic phosphorylation. Geoscience Frontiers, 8(2), 329-335.

Prinz, M., Waggoner, D. G., & Hamilton, P. J. (1980). Winonaites: A primitive achondritic group related to silicate inclusions in IAB irons. In LUNAR AND PLANETARY SCIENCE XI, P. 902-904. Abstract. (Vol. 11, pp. 902-904).

Prior, G. T. (1916). On the genetic relationship and classification of Meteorites. Mineralogical magazine and journal of the Mineralogical Society, 18(83), 26-44.

Rinaudo, C., Cairo, S., Gastaldi, D., Gianfagna, A., Tagliani, S. M., Tosi, G., & Conti, C. (2006). Characterization of fluoro-edenite by μ-Raman and μ-FTIR spectroscopy. Mineralogical Magazine, 70(3), 291-298.

Sack, R. O., & Ghiorso, M. S. (1989). Importance of considerations of mixing properties in establishing an internally consistent thermodynamic database: thermochemistry of minerals in the system Mg2SiO4-Fe2SiO4-SiO2. Contributions to Mineralogy and Petrology, 102(1), 41-68.

Shendrik R.Y., Plechov P.Y., Smirnov S.Z. ArDI – the system of mineral vibrational spectroscopy data processing and analysis, New Data on Minerals, 58 (2024) p. 26-35, doi: 10.25993/FM.2024.58.2024.008

Schulz, T., Münker, C., Mezger, K., & Palme, H. (2010). Hf–W chronometry of primitive achondrites. *Geochimica et Cosmochimica Acta, 74(5)*, 1706-1718.

Stephant, A., Carli, C., Anand, M., Néri, A., Davidson, J., Pratesi, G., ... & Franchi, I. A. (2023). Tissemouminites: A new group of primitive achondrites spanning the transition between acapulcoites and winonaites. *Meteoritics & Planetary Science, 58(1),* 111-134.

Thiemens, M. H., & Heidenreich III, J. E. (1983). The mass-independent fractionation of oxygen: A novel isotope effect and its possible cosmochemical implications. Science, 219(4588), 1073-1075.

Yasutake, M., & Yamaguchi, A. (2017). Multistage formation processes in the acapulcoite-lodranite parent body: Mineralogical study of anomalous lodranite, Yamato 983119. Polar Science, 14, 49-59.

Waeselmann, N., Schlüter, J., Malcherek, T., Della Ventura, G., Oberti, R., & Mihailova, B. (2020). Nondestructive determination of the amphibole crystal-chemical formulae by Raman spectroscopy: One step closer. Journal of Raman Spectroscopy, 51(9), 1530-1548.

Weisberg, M. K., Prinz, M., Clayton, R. N., Mayeda, T. K., Grady, M. M., Franchi, I., ... & Kallemeyn, G. W. (1996). The K (Kakangari) chondrite grouplet. Geochimica et Cosmochimica Acta, 60(21), 4253-4263.

Zeng, X., Shang, Y., Li, S., Li, X., Wang, S., & Li, Y. (2019). The layered structure model for winonaite parent asteroid implicated by textural and mineralogical diversity. Earth, Planets and Space, 71(1), 38.

Figure legend

Fig 1. General view of the Calate 047 winonaite in thin section: a) cross-polarized light, b) under plane-polarized light, c) reflected light without analyzer.

Fig. 2. Phase distribution within a fragment of thin section FN1110 from the Calate 047 winonaite. Opx – low-Ca pyroxene, Cpx – high-Ca pyroxene, Ol –

olivine, Pl – plagioclase, Ed-F – fluoro-edenite, Fe* – iron hydroxides (terrestrial weathering products), Si – silica.

Fig. 3. BSE image of an amphibole-bearing area. Mineral abbreviations are identical to those in Fig. 2.

Fig. 4. BSE images of relict grains preserved among weathering products: troilite (Tro) (a), schreibersite (Scb) (b), and taenite (Fe,Ni) (c).

Fig. 5. BSE image (left) and phase map (right) of an amphibole-bearing region in the thin section, showing a small plagioclase inclusion (blue in phase map) within a fluor-edenite grain.

Fig. 6. Comparison of Raman spectra of fluoro-edenite from the Calate 047 winonaite with a reference sample from the Fersman Mineralogical Museum (this study) and edenite from the RRUFF database (R050415).

Fig. 7. Fa content (in olivine) and Fs content (in orthopyroxene) for various meteorite types. Meteorites (winonaites and lodranites) in which amphiboles have been described are highlighted in color. Mineral chemical composition data are taken from [Benedix et al., 2005; Carpenter et al., 2021; Floss et al., 2007; Yasutake et al., 2017] and from the MetBull database.

Supplementary tables:

Table S1. Fluoro-edenite compositions

Object	reference	SiO_2	TiO_2	Al_2O_3	Cr_2O_3	FeO	MnO	MgO	CaO	Na_2O	K2O	Cl	F	sum	O=Cl2	O=F2	sum
		wt%															
Calate 047	This study	49.93	0.99	6.35	0.20	0.43		23.05	11.22	4.07	0.49	0.06	4	100.78	0.01	1.68	99.09
Calate 047	This study	49.11	1.11	7.29	0.18	0.58	0.08	22.86	11.11	3.87	0.53	0.04	3.9	100.69	0.01	1.65	99.03
Calate 047	This study	49.38	1.07	7.72	0.24	0.48		22.82	11.36	3.83	0.50	0.07	3.9	101.4	0.02	1.65	99.73
Calate 047	This study	49.06	1.09	7.50	0.22	0.44	0.08	22.82	11.23	3.95	0.52	0.07	3.9	100.89	0.02	1.65	99.23
Calate 047	This study	50.12	0.97	7.66	0.19	0.70		21.83	10.70	3.98	0.67	0.03	3.8	100.68	0.01	1.61	99.06
Calate 047	This study	49.52	1.09	6.74	0.22	0.52		22.82	11.32	3.82	0.50	0.07	3.8	100.44	0.02	1.61	98.82
HaH 193 (winonaite)	Floss et al., 2007	49.70	0.63	5.89	0.38	1.08	0.08	22.80	11.40	3.88	0.45	0.04	4.1	100.38	0.01	1.71	98.67
HaH 193 (winonaite)	Floss et al., 2007	50.00	1.08	5.88	0.62	1.25	0.09	23.30	11.20	4.09	0.48		4.6	102.55	0.00	1.92	100.63
NWA 13432 (winonaite)	Carpenter et al., 2021	50.10	1.00	6.61	0.36	0.77	0.06	23.19	11.76	3.76	0.57	0.07	4.3	102.59	0.02	1.83	100.75
Biancavilla, Catania, Sicily, Italy	Gianfagna and Oberti, 2001	52.92	0.29	3.53		2.50	0.46	22.65	10.83	3.20	0.84	0.07	4.4	101.64	0.02	1.83	99.79

Table S2. Olivine compositions for amphibole-bearing meteorites summarized from literature sources and from this work.

meteorite	reference	SiO_2	Al_2O_3	Cr_2O_3	FeO	MnO	MgO	CaO	NiO	sum	mg#
		wt%									
Calate 047	This study	41.57	0.06	0.04	1.63	0.18	55.51	0.05	0.06	99.1	98.38
Calate 047	This study	41.6	0.03	0	1.61	0.14	55.53	0.06	0.01	99.0	98.40
Calate 047	This study	41.52	0.05	0.04	1.72	0.19	55.52	0.01	0.01	99.1	98.29
Calate 047	This study	41.64	0.04	0	1.7	0.15	55.51	0.06	0.01	99.1	98.31
Calate 047	This study	42.18	0.07	0.01	1.74	0.18	56.4	0.02	0	100.6	98.30
Calate 047	This study	41.78	0.07	0.08	1.64	0.17	55.71	0.01	0.02	99.5	98.38
Calate 047	This study	41.62	0.06	0.01	1.83	0.2	55.93	0	0	99.7	98.20
HaH 193	Floss et al., 2007	41.5			4.41	0.2	53.10			99.23	95.55
HaH 193	Floss et al., 2007	42.10		0.030	4.52	0.31	53.80	0.03		100.79	95.50
Mayo Belwa	Graham et al., 1977	42.7		0.020	0.06		56.30	0.0		99.12	99.94

Table S3. Pyroxene compositions for amphibole-bearing meteorites summarized from literature sources and from this work.

meteorite	type	reference	SiO_2	TiO_2	Al_2O_3	Cr_2O_3	FeO	MnO	MgO	CaO	Na_2O	sum	mg#	Wo %	En %	Fs %
			wt%													
Calate 047	Opx	This study	58.31	0.12	0.48	0.15	1.21	0.27	38.00	0.85	0.04	99.43	98.25	1.55	97.26	0.78
Calate 047	Opx	This study	58.48	0.10	0.47	0.11	1.25	0.20	38.03	0.89	0.04	99.57	98.19	1.62	97.08	1.00
Calate 047	Opx	This study	57.62	0.16	1.83	0.13	1.22	0.27	37.49	0.92	0.01	99.65	98.21	1.70	96.86	1.04
Calate 047	Opx	This study	57.97	0.16	2.00	0.09	1.31	0.24	37.98	0.80	0.04	100.59	98.10	1.46	97.73	0.44
Calate 047	Opx	This study	57.72	0.14	0.96	0.13	1.29	0.26	37.49	0.90	0.02	98.91	98.11	1.66	96.78	1.17
Calate 047	Opx	This study	58.45	0.12	0.70	0.18	1.31	0.18	38.13	0.84	0.02	99.93	98.11	1.53	97.23	0.97
Calate 047	Cpx	This study	54.09	0.48	1.56	0.17	0.48	0.18	19.04	22.43	0.39	98.82	98.61	45.37	53.62	0.70
Calate 047	Cpx	This study	53.92	0.39	2.11	0.18	0.49	0.13	19.00	22.35	0.36	98.93	98.57	45.36	53.65	0.78
Calate 047	Cpx	This study	54.02	0.46	1.95	0.20	0.60	0.16	18.96	22.30	0.43	99.08	98.26	45.26	53.64	0.77
Calate 047	Cpx	This study	53.92	0.65	2.90	0.19	0.53	0.16	18.85	22.30	0.43	99.93	98.45	45.45	53.45	0.84
Calate 047	Cpx	This study	54.23	0.61	1.48	0.26	0.63	0.14	18.89	22.73	0.42	99.39	98.16	45.81	53.07	0.80
Calate 047	Cpx	This study	54.83	0.58	1.13	0.17	0.59	0.11	18.98	22.62	0.41	99.42	98.29	45.63	53.27	0.93
HaH 193 (winonaite)	Opx	Floss et al., 2007	58.60	0.14	0.28	0.18	3.24	0.26	36.30	0.96	0.05	100.01	95.23	1.77	93.18	4.67
HaH 193 (winonaite)	Opx	Floss et al., 2007	58.50	0.20	0.29	0.20	3.64	0.32	36.50	1.36		101.01	94.70	2.46	92.78	4.28
Abee (EH4)	Opx	Rubin and Keil., 1983	59.80		0.08		0.95		39.00	0.09		99.92	98.65	0.16	98.49	1.35
Abee (EH4)	Opx	Rubin and Keil., 1983	59.90				0.80		39.70	0.09		100.49	98.88	0.16	98.80	1.03
Abee (EH4)	Opx	Rubin and Keil., 1983	59.60		0.16		1.16		39.00	0.10	0.09	100.11	98.36	0.18	98.18	1.64
Abee (EH4)	Opx	Rubin and Keil., 1983	60.10		0.07		0.87		39.60	0.09		100.73	98.78	0.16	98.62	1.22
Abee (EH4)	Opx	Rubin and Keil., 1983	59.60		0.06		0.51		39.00	0.08		99.25	99.27	0.15	99.13	0.73
Abee (EH4)	Opx	Rubin and Keil., 1983	59.90				0.71		39.60	0.08		100.29	99.00	0.14	98.86	0.99
Abee (EH4)	Opx	Rubin and Keil., 1983	59.50		0.17		0.64		38.70	0.40	0.08	99.49	99.08	0.73	98.36	0.91

Abee (EH4)	Opx	Rubin and Keil., 1983	59.50		0.11		1.30		38.10	0.62		99.63	98.12	1.13	97.01	1.86
Mayo Belwa (aubrite)	Opx	Graham et al., 1977	59.00		0.07		0.02		39.30	0.32		98.71	99.97	0.58	99.39	0.03

Table S4. Plagioclase compositions for amphibole-bearing meteorites summarized from literature sources and from this work.

meteorite	reference	SiO_2	Al_2O_3	FeO	MgO	CaO	Na_2O	K_2O	sum	An %	Ab %	Or %
		wt%								molar		
Calate 047	This study	61.85	23.77	0.36	0.05	3.84	8.79	0.50	99.16	18.81	77.93	2.92
Calate 047	This study	62.13	23.99	0.24	0.07	3.79	8.82	0.48	99.52	18.56	78.16	2.80
Calate 047	This study	61.84	24.18	0.23	0.02	3.57	8.89	0.40	99.13	17.71	79.79	2.36
Calate 047	This study	61.67	24.94	0.32	0.09	3.67	8.77	0.45	99.91	18.17	78.56	2.65
Calate 047	This study	62.23	23.62	0.48	0.08	3.69	8.82	0.48	99.40	18.15	78.49	2.81
HaH 193 (winonaite)	Floss et al., 2007	61.9	23.3	0.19		4.44	8.92	0.4	99.15	21.09	76.65	2.26
HaH 193 (winonaite)	Floss et al., 2007	62.7	22	0.27		4.32	9.13	0.4	98.82	20.27	77.50	2.23
Mayo Belwa (aubrite)	Graham et al., 1977	65.5	19.9			1.87	10.4	0.47	98.14	8.80	88.57	2.63